Some recent advances of shock wave physics research at the Laboratory for Shock Wave and Detonation Physics Research

2002 J. Phys.: Condens. Matter 14 10799

(http://iopscience.iop.org/0953-8984/14/44/380)

INSTITUTE OF PHYSICS PUBLISHING JOURNAL OF PHYSICS: CONDENSED MATTER

J. Phys.: Condens. Matter **14** (2002) 10799–10808 PII: S0953-8984(02)38108-6

Some recent advances of shock wave physics research at the Laboratory for Shock Wave and Detonation Physics Research

Fuqian Jing and Hua Tan

Laboratory for Shock Wave and Detonation Physics Research, Southwest Institute of Fluid Physics, PO Box 919-111, Mianyang, Sichuan 621900, China

Received 13 June 2002
Published 25 October 2002
Online at stacks.iop.org/JPhysCM/14/10799

Abstract

Progress made in recent years on three topics that have been investigated at the Laboratory for Shock Wave and Detonation Physics Research are presented in this report. (1) A new equation of state (EOS) has been derived which can be used from a standard state to predict state variable change along an isobaric path. Good agreements between calculations for some representative metals using this new EOS and experiments have been found, covering a wide range from hundreds of MPa to hundreds of GPa and from ambient temperature to tens of thousands of GPa. (2) An empirical relation of $Y/G =$ constant (Y is yield strength, G is shear modulus) at HT–HP has been reinvestigated and confirmed by shock wave experiment. 93W alloy was chosen as a model material. The advantage of this relation is that it is beneficial to formulate a kind of simplified constitutive equation for metallic solids under shock loading, and thus to faithfully describe the behaviours of shocked solids through hydrodynamic simulations. (3) An attempt at microstructure characterization for a failure wave in shocked glass has been carried out for the first time. Analyses on both the fractal dimension of the cracks' propagating path and the degree of damage in the failed region qualitatively revealed that *ZF1* glass has a much less damaged structure than $K9$ glass at nearly the same loading stress. Based on the above analysis, we conjecture inhomogeneous immiscible phases, more in $K9$ than in *ZF1*, distributed in the glass body of the intrinsic factor, exhibiting as numerous locally strained spots due to the shock induced different compressibilities between the matrix and the immiscible phases. When the surface cracks, activated by the shearing action of one-dimensional strain loading, propagate and arrive at the strained spot boundaries, new cracks would be generated, accompanied by crack turning and branching, and thus cause glass body fracturing and fragmenting. In other words, the more numerous the strained spots are, the more severely damaged the structure of the shocked glass.

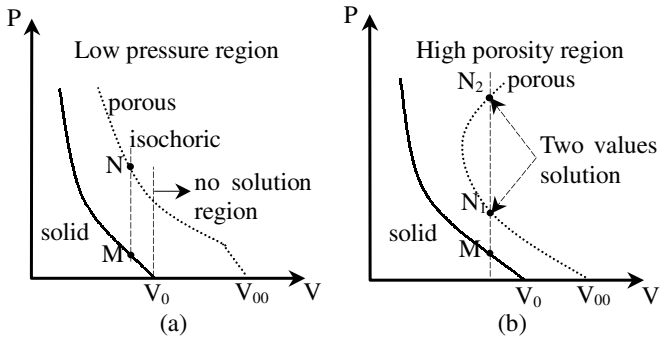

Figure 1.

1. A new equation of state

Traditionally, the Grüneisen equation of state (EOS) is acknowledged to be useful to estimate thermodynamic variable change from a standard state along an isochoric path. However, two problems always trouble us when the Grüneisen EOS is utilized to perform such a estimation for porous material. The first problem occurs in the lower pressure region (see figure 1(a)). If point N is located within $V > V_0$, no solution is obtained since in most cases we have no standard data on point M to be used for such estimations. The second problem occurs in the high porosity case ($\alpha_0 = V_{00}/V_0 > 2$ in general; see figure 1(b)). In this case the porous Hügoniot may exhibit 'expansion' behaviour and thus a two-valued solution (N_1 and N_2) will emerge.

To solve these difficulties, we think a better way is to find a new EOS that can make this estimation along an isobaric path. For this reason, Wu and Jing [1, 2] proposed an EOS of this kind based on thermodynamic considerations and obtained good predictions for porous materials within a pressure range up to hundreds of GPa, with success especially in the lower porosity case ($\alpha_0 < 2$ in general) and the elastic–plastic behaviour around hundreds of MPa. Later, Geng [3] gave a statistical mechanics description for this new EOS and obtained good predication for porous materials, with success especially in the higher porosity case ($\alpha_0 > 2$) and the 'expansion' behaviour description.

The mathematical expression of this EOS is

$$V - V_C = \frac{R}{p}(H - H_C) \tag{1}$$

or

$$V_T = \frac{R}{p}H_T \tag{2}$$

where V is specific volume, p pressure and H specific enthalpy. The subscripts C and T are respectively the cold and thermal contributions. R is a material constant which is connected with some other physical properties by the relation

$$R = p\left(\frac{K_T}{K_S}\right)\frac{\alpha}{\rho C_V}, \qquad \text{(from thermodynamic consideration)} \tag{3}$$

or

$$R = \left(\frac{\partial \ln \Theta}{\partial \ln p}\right)_T, \qquad \text{(from statistical mechanics consideration)} \tag{4}$$

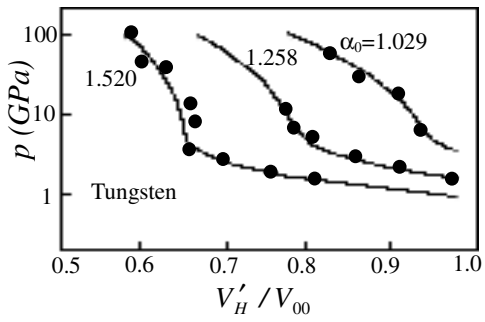

Figure 2.

where K_T is the isothermal bulk modulus, K_S the isentropic bulk modulus, a the volume expansion coefficient, ρ the density, C_V the specific heat at constant volume and Θ the Debye temperature.

To predicate the Hügoniot of porous material from a solid Hügoniot standard, a basic equation was derived based on this new EOS together with the enthalpy and the Rankine–Hügoniot relation, written as [1, 2]

$$V'_H = aV_H + b(V_1 - V_0) + c(V'_C - V_C) + \mathrm{d}V_{00} \tag{5}$$

where

$$a = \left(1 - \frac{R}{2}\right)\Big/\beta, \qquad b = \left(\frac{R}{2}\right)\Big/\beta, \qquad c = (1-R)/\beta,$$
$$d = b\left(\frac{p_1}{p}\right), \qquad \beta = 1 - \left(\frac{R}{2}\right)\Big/\left[1 - \left(\frac{p_1}{p}\right)\right]$$

$V'_H$and V_H represent Hügoniot specific volumes of porous and solid materials, respectively, and V'_C and V_C represent respectively cold specific volumes of porous and solid ones. The subscript 1 denotes the Hügoniot elastic limit of the porous material.

With equation (5), we can calculate V'_H from V_H providing V_C, V'_C, p_1 and V_1 are all known. For this reason, we take the Born–Mayer potential [4] to relate V_C to p and the Carrol–Holt model [5] to relate V'_C, p_1 and V_1 to p. Good agreements, over a wide range from hundreds of MPa to hundreds of GPa, between calculations and experiments for 2024 Al, Cu, Fe and W have been found in the case of $\alpha_0 < 2$. Figure 2 gives the data of porous W as an example to demonstrate the good capability of equation (5).

The situation would be changed for $\alpha_0 > 2$, because a large temperature increase in shocked porous material would be generated and, therefore, the anharmonic oscillator model and thermal electron contribution should be introduced in the computations. Consequently, equation (5) might be modified and expressed as [3]

$$V'_H = V_{H,L} + \frac{R}{2-R}(V_{00} - V_0) + \frac{\beta_0}{4p}\left(\frac{V_{H,L}}{V_{0K}}\right)^{1/2} T^2; \tag{6}$$

the first term on the right-hand side represents the lattice contribution while the third term the thermal electron contribution. We combine equation (6) with the following equations:

$$p = \rho_0 C_0^2 \eta/(1-\lambda\eta)^2 \tag{7}$$

$$\frac{\mathrm{d}T}{\mathrm{d}p} - \frac{R'}{p}T = \frac{1}{2C'_p}(V_0 - V'_H) + p\frac{\mathrm{d}V'_H}{\mathrm{d}p} \tag{8}$$

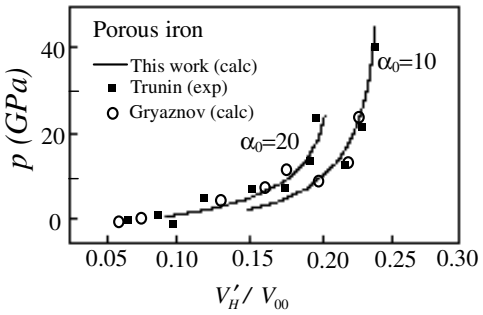

Figure 3.

where

$$\eta = 1 - (V_H/V_0) \tag{9}$$

$$R' = R/(1+3R) \tag{10}$$

$$C'_p = \frac{C_{p0}}{2}[1 + (1+Z)^{-2}] + \frac{3}{2}\beta T \tag{11}$$

in which R' and C'_p are effective values of R and C_p consisting of the thermal electron contribution besides the lattice contribution, respectively. $Z = lRT/\mu C_x^2$ is called the deviation degree from solid state, where R is the gas constant, μ the molar mass, C_x the cold sound velocity and l the anharmonic parameter. C_0 and λ are two constants involved in the shock velocity equation $D = C_0 + \lambda u$ (D is the shock velocity and u the particle velocity).

With the help of equations (6)–(11), Hügoniots of porous Cu, Fe and W were computed. Good agreements between calculations and experiments were also obtained over a wide range at pressures up to nearly 200 GPa and with α_0 values up to 20. Figure 3 gives the data on porous Fe as an example to show the good capability of equation (6). The unique feature of this new EOS is that it is capable of predicting well the porous Hügoniot from a solid standard on the basis of a unified theoretical framework; besides, it is valid for a wide range as mentioned above.

2. An empirical relation Y/G = constant for metals

In certain cases, knowledge of yield strength $Y(p,T)$ and shear modulus $G(p,T)$ are of significance in hydrodynamic simulations. Determination of $Y(p,T)$ is more difficult than that of $G(p,T)$, and therefore to find a handy way for determining $Y(p,T)$ is very important to us. For this problem, two events should be noticed. In 1975, Chau and Rouff [6] claimed they had conducted a hydrostatic experiment and found an empirical relation

$$Y(p)/G(p)|_{77\,\mathrm{K}} = \text{constant} \tag{12}$$

that is valid up to 5 GPa, i.e. $Y(p,T)$ could be determined from $G(p,T)$ through equation (12). The second event is that, in 1980, Steinberg *et al* [7] proposed two simplified constitutive equations used for simple metallic solids

$$G = G_0\left[1 + \frac{G'_p}{G_0}p + \frac{G'_T}{G_0}(T-300)\right] \tag{13}$$

$$Y = Y_0\left[1 + \frac{Y'_p}{Y_0}p + \frac{Y'_T}{Y_0}(T-300)\right]. \tag{14}$$

Clearly, the above two expressions are, in essence, series expansions and truncated at their first partial derivatives separately for $G(p, T)$ and $Y(p, T)$. Six unknowns (G_0, Y_0, G'_p, G'_T, Y'_p and Y'_T) should be predetermined so as to make equations (13) and (14) possible for applications. To diminish the difficulty in determinations of unknowns, they directly adopted the assumption of $Y(p, T)/G(p, T) =$ constant without any verification, yielding

$$(G'_p/G_0) = (Y'_p/Y_0), \qquad (G'_T/G_0) = (Y'_T/Y_0). \tag{15}$$

By using equation (15), the number of unknowns in Steinberg's constitutive equations can be reduced from six to four (G_0, Y_0, G'_p and G'_T). They used the above approach to describe the elastic–plastic properties at HT–HP for metals and obtained successful results in their hydrodynamic simulations, as compared with experiments. This fact would be regarded as indirect evidence for the applicability of $Y(p, T)/G(p, T) =$ constant relation.

A further problem would be raised: whether the validity of $Y(p, T)/G(p, T) =$ constant extended from equation (12) could be directly verified by experiment over a wide p and T range, and whether this extended relation could be also valid for multiphase alloys, since Steinberg's investigations are mostly for simple metals. For this reason, we chose 93W alloy (consisting of 93% W as matrix and 7% Fe–Ni–Co as binder) as a model two-phase alloy to conduct this verification. Many methods could be utilized to measure the value of G_0, Y_0, G'_p and G'_T.

Some recommended data obtained from different methods for 93W alloy are given below:

$$G_0 = 132 \text{ GPa}, \qquad G'_p = 1.794, \qquad G'_T = -0.0161 \text{ GPa}/^\circ$$

(from supersonic method [8])

$$K_0 = 270 \text{ GPa}, \qquad K'_p = 4.108$$

(from Hügoniot measurement [9])

$$Y_0 = 1.4 \text{ GPa}$$

(from shock stress measurement [10])

$$G'_T = -0.04 \text{ GPa}/^\circ$$

(from $G(p_H)$ measurement and $G(p_S)$ calculations).

It should be noticed that the values of G'_T obtained separately from supersonic and from $G(p_H)$ and $G(p_S)$ methods are very different. We chose the latter as a final recommendation since it was obtained in a much wider temperature range as compared with supersonic means. Some of the experimental details will be given below.

The experimental sound velocity data versus shock pressures (p_H) are drawn in figure 4. Obviously, these data can be classified as two linear fits. The upper one represents longitudinal sound velocity because it passes through the supersonic longitudinal velocity datum. This fit may be expressed by

$$C_l = 5.45 + 0.013 p_H - 2.24 \times 10^{-5} p_H^2. \tag{16}$$

The lower one is the calculated bulk wave velocity, C_b, curve, with which two experimental data closely coincide. Based on the above two fits, $G(p_H)$ would be calculated by using the relation of $G = (4/3)\rho(C_l^2 - C_b^2)$, thus yielding

$$G(p_H) = 110.4 + 2.18 p_H - 7.62 \times 10^{-3} p_H^2. \tag{17}$$

Equation (17) has two applications. One is used to calculate G'_T, for which $G(p_S)$ should be calculated first. $G(p_S)$ is the G value along an isentropic compression locus and could be computed through the Birch–Murnaghan EOS

$$G(p_S) = (1 + 2f)^{2/5}(a_0 + a_1 f + a_2 f^2) \tag{18}$$

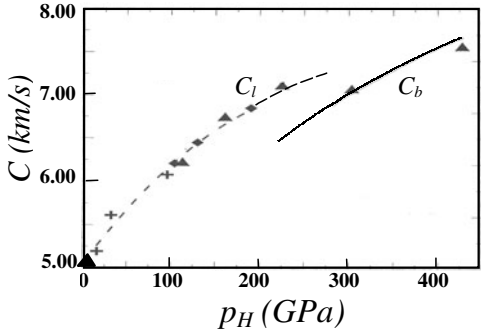

Figure 4.

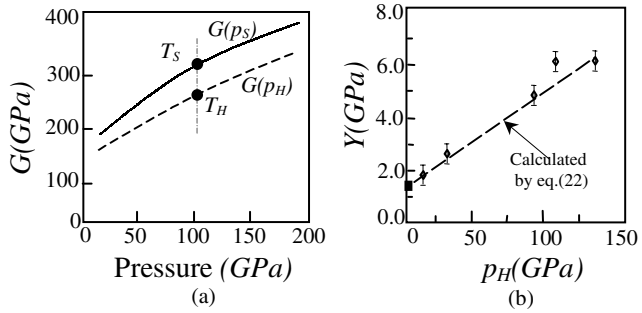

Figure 5.

where

$$a_0 = G_0, \qquad a_1 = 3K_0G'_p - 5G_0,$$
$$a_2 = \frac{9}{2}\left\{K_0^2\left[G''_p + (K'_p - 4)\frac{G'_p}{K_0}\right] + \frac{35G_0}{4}\right\}$$
$$f = \tfrac{1}{2}[(\rho/\rho_0)^{2/3} - 1].$$

There are five parameters (G_0, G'_p, G''_p, K_0 and K'_p) that are needed to perform $G(p_S)$ calculations. Among them, G_0, G'_p, K_0 and K'_p have been recommended before; $G''_p = -0.033\ \mathrm{GPa}^{-1}$ has been approximately calculated from *ab initio* calculation by us [11]. Figure 5(a) shows $G(p_H)$ and $G(p_S)$ curves. For each pressure point, the corresponding T_H and T_S could be computed respectively by the formulae

$$T_H = \mathrm{e}^{-\int_{V_0}^{V_H}\frac{\gamma}{V}\,\mathrm{d}V}\left\{\int_{V_0}^{V_H}\frac{1}{2C_V}\left[p + (V_0 - V_H)\frac{\mathrm{d}p_H}{\mathrm{d}V}\right]\mathrm{e}^{\int_{V_0}^{V_H}\frac{\gamma}{V}\,\mathrm{d}V + T_0}\right\} \tag{19}$$

$$T_S = T_0\exp(\gamma_0\eta). \tag{20}$$

Interestingly, with this approach G_H and G_S at any pressure can be well described by

$$G_H = G_S - 0.04(T_H - T_S) \qquad \text{or} \qquad G'_T = -0.04\ \mathrm{GPa}/^\circ. \tag{21}$$

Obviously, this value of G'_T is valid for a wide range covering 0–150 GPa and ambient temperature to thousands of kelvin.

The second use of $G(p_H)$ is to verify whether the relation of $Y(p_H)/G(p_H) =$ constant holds at HT–HP. The measured data of $Y(p_H)$ are plotted in figure 5(b) together with a dotted

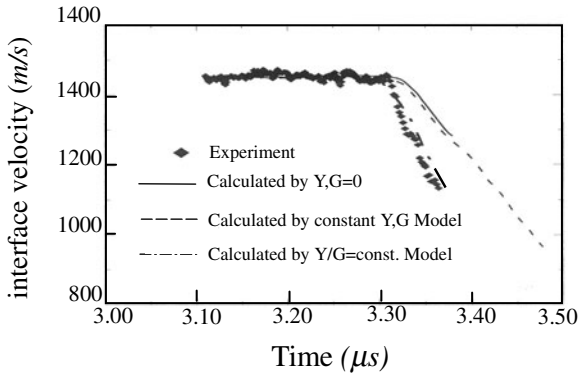

Figure 6.

line calculated by

$$Y(p_H) = (Y_0/G_0)(110.4 + 2.18p_H - 7.62 \times 10^{-3} p_H^2). \tag{22}$$

Please note that the expression in brackets is just the same as the $G(p_H)$ expression, equation (17). That is to say, the relation of

$$Y(p_H)/G(p_H) = \text{constant} \tag{23}$$

holds within the same range as the calculated G'_T does. It should be noticed that equation (23) only holds good for Hügoniot states, not for off-Hügoniot states, while this is the case we always meet with in hydrodynamic simulations. So, we should further verify whether equation (23) could be extended as the relation $Y(p, T)/G(p, T) = \text{constant}$.

This task has been performed by comparing hydrodynamic calculation, using different constitutive models, with an experimental interface velocity history record. This is only an indirect approach of course. The results are plotted in figure 6. It demonstrates that the relation of $Y(p, T)/G(p, T) = \text{constant}$ is indeed a better constitutive description for 93W, a two-phase metallic alloy.

3. Microstructure characterization for the failure wave in shocked glass

In the past, investigations on the failure wave in shocked glass mainly emphasized failure wave velocity variations with loading stress [12, 13], and using it to analyse the mechanism responsible for failure wave generation [12, 14]. When the loading stress is lower than the Hügoniot elastic limit of the glass being studied, common knowledge of the failure mechanism is ascribed to the surface microcracks development model [15, 16]. An attempt to perform microstructure characterization for the region behind the failure front has been performed for the first time at the Laboratory for Shock Wave and Detonation Physics Research (LSD), with $K9$ and *ZF1* glass as sample materials.

Figure 7 shows two experimental free surface velocity profile records of $K9$ glass at different loading stresses. The 'recompression' indicates the failure wave existing in the shocked glass. From the recompression arrival time one can calculate the failure wave velocity, V_f (see table 1), while from the recompression signal amplitude one can calculate the acoustic impedance ratio of the failed region to the compressed region, and thus assess the degree of damage of the failed layer.

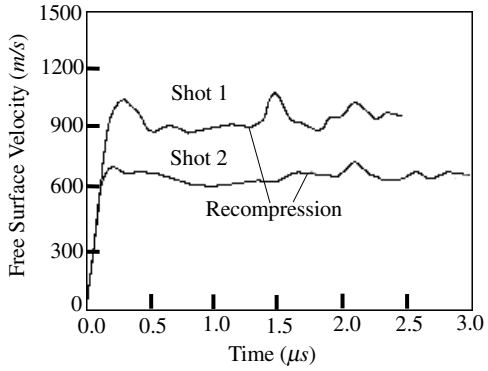

Figure 7.

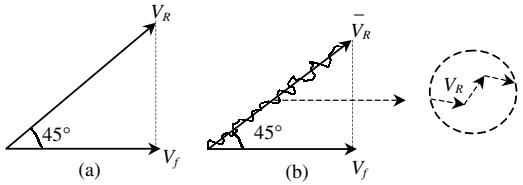

Figure 8.

Table 1. Failure wave velocities of *K*9 and *ZF1* glasses.

Shot no	Sample glass	Loading stress (GPa)	Failure wave velocity, V_f (km s^{-1})	Fractal dimension D
1	*K*9	5.34	0.82	1.240
2	*K*9	8.02	1.37	1.128
3	*ZF1*	5.15	1.06	1.093

3.1. Geometrical description for the crack propagating path

Rosorenov *et al* [12] proposed that the failed layer is a zone with a network of cracks, which propagate forward in a manner analogous to mode II fracture, with a limiting crack velocity V_R the same as the shear wave velocity V_T. The measured V_T are 3.70 km s^{-1} for *K*9 glass and 2.40 km s^{-1} for *ZF1* glass. As shown in figure 8(a), supposing the ideal crack propagating path is a straight line at 45° with respect to the shock stress direction, the observed failure wave velocity V_R would be ∼2.62 km s^{-1} for *K*9 and ∼1.75 km s^{-1} for *ZF1*. These two predications are much higher than the observed values (see table 1).

To explain the observed lower measured V_f value, we suggest the crack propagating path is probably a zigzag route rather than a straight one, and then an effective $\bar{V}_R$ should be proposed as the macroscopic crack propagating velocity (see figure 8(b)). Moreover, the roughness of the crack path was further analysed by using fractal geometry theory through fractal dimension, D, analysis [17, 18].

$$\bar{V}_R = V_R \Big/ \left(\frac{\Delta\bar{a}}{a}\right)^{D-1}$$

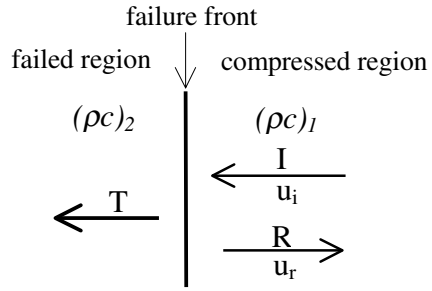

Figure 9.

Table 2. Degree of damage of the failed region for shocked *K*9 and *ZF1* glasses.

Shot no	u_{fs1} (m s^{-1})	u_{fs2} (m s^{-1})	n (%)	n' (%)	Damage parameter (N)
1	642	700	83.4	70.9	0.570
2	915	1000	83.0	70.9	0.584
3	655	665	97.0	72.8	0.041

where $0 \leqslant \left(\frac{\Delta\bar{a}}{a}\right) \leqslant 1$ is the microstructure parameter of the fracture surface. $D = 1$ corresponds to an ideal smooth path, while $1 < D < 2$ a zigzag path. For the glassy material under dynamic loading, the typical value of $\left(\frac{\Delta\bar{a}}{a}\right)$ is ∼0.01. The calculated D values for shot numbers 1, 2 and 3 are also listed in table 1, demonstrating that the D value decreases with increasing loading stress for a given glass; on the other hand, as compared with *K*9, *ZF1* glass has a lower D at nearly the same loading stress, which indicates that the crack propagating paths are smoother in *ZF1* than in *K*9 glass.

3.2. Degree of damage analysis for the failed region

As shown in figure 9, an acoustic wave propagating in inhomogeneous materials will be reflected and transmitted when it meets a boundary separated by different acoustic impedance materials. In this case, the acoustic impedance ratio of the failed layer to the compressed region is

$$n = \frac{(\rho c)_2}{(\rho c)_1} = 2\frac{u_{fs1}}{u_{fs2}} - 1$$

where u_{fs1} and u_{fs2} are determined from the measured V_{fs} amplitudes before and after the recompression arrival on the profile record (see figure 7). The calculated values of n are given in table 2.

On the other hand, the lowest value of n, denoted by n', should be regarded as the failed layer behaving as a fluid-like state with an acoustic velocity the same as the bulk sound velocity C_b, then yielding

$$n' \cong C_b/C_{10}$$

where C_{10} is the longitudinal acoustic wave velocity. Then the values of n' are 0.709 for *K*9 and 0.728 for *ZF1* glass, respectively.

A degree of damage, N, is introduced and defined as

$$N = (1 - n)/(1 - n')$$

where $N = 0$ corresponds to the undamaged layer, while $N = 1$ to the completely damaged layer. The calculated values of N are also given in table 2, which demonstrates that *ZF1* has a much lower degree of damage than $K9$ glass at nearly the same loading stress.

From the above analyses, we are informed from both the fractal dimension of the crack propagating path and the degree of damage in the failed region that the microstructure of the shocked glass is strongly dependent on the material being studied. For this circumstance, we conjecture that the inhomogeneous immiscible phases containing in the glass body, which are more numerous in $K9$ than in *ZF1* glass, play an intrinsic role and show up as numerous locally strained spots due to the shock induced different compressibilities between the matrix and inhomogeneous immiscible phases. When the raw cracks existing on the impacted surface, activated by the shear under one-dimensional strain loading, propagate and arrive at the strained spot boundaries, new cracks would be generated, accompanied by crack turning and branching, and thus propagate forward. To sum up, the more numerous the spots, the more severely damaged the microstructure of the shocked glass.

References

[1] Wu Q and Jing F Q 1995 *Appl. Phys. Lett.* **67** 49
[2] Wu Q and Jing F Q 1996 *J. Appl. Phys.* **80** 4343
[3] Geng H Y 2001 *Master Dissertation CAEP* (in Chinese)
[4] See, for example,
Zharkov V N and Kalinin V 1971 *Equation of State for Solids at High Pressures and Temperatures* (New York: Consultants Bureau) p 217
[5] Carroll M M and Holt A C 1972 *J. Appl. Phys.* **43** 1626
[6] Chua J O and Ruoff A L 1975 *J. Appl. Phys.* **46** 4659
[7] Steinberg D J *et al* 1980 *J. Appl. Phys.* **51** 1498
[8] Shen Z Y 1997 *Technical Report LSD*
[9] Wang J G and Shi W F 1995 *Chin. J. High Pressure Phys.* **9** 195 (in Chinese)
[10] Zhang W J *et al* 1995 *Chin. J. High Pressure Phys.* **15** 44 (in Chinese)
[11] Hua J S *et al* 2000 *Acta Phys. Sin.* **49** 2443 (in Chinese)
[12] Rasorenov S V *et al* 1991 *High Pressure Res.* **6** 225
[13] Bourne N K *et al* 1996 *J. Appl. Phys.* **80** 4328
[14] Clifton R J 1993 *Appl. Mech. Rev.* **46** 540
[15] Bourne N *et al* 1997 *J. Appl. Phys.* **81** 6670
[16] He H L *et al* 1997 *Chin. Phys. Lett.* **14** 538
[17] Takahash K and Arakawa K 1987 *Exp. Mech.* **33** 922
[18] Xie H 1989 *Int. J. Fracture* **41** 267